Biomechanical stress analysis of Type-A aortic dissection at pre-dissection, post-dissection and post-repair states

Christina Sun[1], Tongran Qin[1], Asanish Kalyanasundaram[2],
John Elefteriades[2], Wei Sun[1], and Liang Liang[3]

[1] Sutra Medical Inc, Lake Forest, CA, USA
[2] Aortic Institute at Yale-New Haven Hospital, Yale University School of Medicine, New Haven, CT, USA
[3] Department of Computer Science, University of Miami, Coral Gables, FL, USA

biorxiv

* Address for correspondence
Liang Liang, PhD
Department of Computer Science
University of Miami
Coral Gables, FL, USA
Tel: 3052848381

ABSTRACT

Acute type A aortic dissection remains a deadly and elusive condition, with risk factors such as hypertension, bicuspid aortic valves, and genetic predispositions. As existing guidelines for surgical intervention based solely on aneurysm diameter face scrutiny, there is a growing need to consider other predictors and parameters, including wall stress, in assessing dissection risk. Through our research, we aim to elucidate the biomechanical underpinnings of aortic dissection and provide valuable insights into its prediction and prevention.

We applied finite element analysis (FEA) to assess stress distribution on a rare dataset comprising computed tomography scans obtained from eight patients at three stages of aortic dissection: pre-dissection (preD), post-dissection (postD), and post-repair (postR). Our findings reveal significant increases in both mean and peak aortic wall stresses during the transition from the preD to postD state, reflecting the mechanical impact of dissection. Surgical repair effectively restores aortic wall stresses to pre-dissection levels across all regions, suggesting its effectiveness in mitigating biomechanical stress. Furthermore, we identified stress concentration regions within the aortic wall that closely correlated with observed dissection borders, offering insights into high-risk areas.

This study demonstrates the importance of considering biomechanical factors when assessing aortic dissection risk. Despite some limitations such as uniform wall thickness assumptions and the absence of dynamic blood flow considerations, our patient-specific FEA approach provides valuable mechanistic insights into aortic dissection. These findings hold promise for improving predictive models and informing clinical decisions to enhance patient care.

Keywords: **aortic dissection, finite element analysis, stress analysis**

.

1. INTRODUCTION

Type A aortic dissection, a rare but catastrophic cardiovascular event, poses a significant clinical challenge due to its high mortality and morbidity rate.[1] It is initiated by the development of a tear in the intima of the aorta, which allows pressurized blood to enter the aortic wall, subsequently leading to the separation of aortic wall layers. This condition can compromise branch vessel inflow, cause lumen compression, and result in severe complications such as acute aortic valve regurgitation, myocardial infarction, stroke, visceral organ ischemia, or frank aortic rupture.[1,2]

Dissections of the ascending aorta (Type A) are both more common and significantly more dangerous than descending aortic dissections (Type B). Approximately 60% of aortic dissections are Type A.[1,3] If left untreated, the mortality rate of TAAD patients is increases 1-2% every hour for the first 48 hours and up to 68% within the first two days,[4,5] whereas the overall in-hospital mortality rate of Type B aortic dissection patients is 11% in a month.[1,6] While certain risk factors, such as hypertension, bicuspid aortic valves, and genetic predispositions like Marfan syndrome have been identified,[2,7,8] the precise triggers of TAAD initiation remain elusive.

One commonly employed American and European guideline for mitigating the risk of aortic dissection is the prophylactic surgical replacement of the ascending aorta when an aneurysm reaches a diameter of 5.5 centimeters.[9,10] However, large retrospective studies have cast doubt on the effectiveness of this guideline, suggesting that it may be an inadequate predictor.[11,12] From an engineering perspective, aortic dissection can be viewed as a biomechanical failure of the aortic wall, occurring when wall stress exceeds wall strength.[13,14]

Computational modeling has emerged as a valuable tool for studying ascending aortic aneurysms, yet the current computational studies have not been able to precisely determine when and where the

dissection would occur, limiting their predictive power for clinical use. To understand the biomechanical aspects of aortic dissection, studies have explored factors associated with wall shear stress and wall principal stress, and their impact on the aortic wall structural integrity. Bäumler et al. presented a computational framework for simulating aortic dissection, considering factors like vessel wall deformation, blood flow, and pressure in patient-specific models, concluding that the flexibility of the dissection membrane significantly affects local blood flow patterns.[15] A study by Martufi et al. quantitatively characterized the geometry of abdominal aortic aneurysms using CT data, proposing that various geometric indices such as size, shape, and curvature-based metrics may be necessary to evaluate the risk of rupture.[16] He et al. utilized machine learning to predict the local strength of ascending thoracic aortic aneurysm tissues based on tension-strain data, suggesting that early phase response features can reliably estimate tissue strength.[17] Research by Nathan et al. explored the relationship between regional wall stress and aortic dissections, notably near the sinotubular junction and the left subclavian artery, suggesting a potential role in the pathogenesis of aortic dissections.[18]

One limitation of previous studies is the lack of a complete longitudinal data sets which cover a patient's pre-dissection state, post dissection state, and after surgical repair state, which are difficult to obtain from clinics. Moreover, engineering analysis of these patient-specific aortic wall mechanics often require the patient-specific material properties of these patients.

This research paper aims to contribute to the understanding of aortic dissection by investigating the change in aortic stress distributions at different time points. By assessing aortic stress distributions using noninvasive imaging techniques and finite element analysis, we seek to reveal increased peak and mean stress in patients who have sustained acute type A aortic dissection. Importantly, we possess a rare dataset that includes pre-dissection (preD), post-dissection (postD), and post-repair (postR) data

from the same patients, allowing for paired t-test analyses across these time points. This comprehensive dataset sets our research apart from existing studies in the field.

2. METHODS

2.1 Patient clinical data

As seen in Table 1, clinical data from eight patients between the age of 41 and 75 were collected retrospectively from Yale New Haven Hospital. An engineering analysis was conducted on this rare dataset comprising of retrospectively obtained computed tomography (CT) scans. The dataset included pre-dissection (PreD) and post-dissection (PostD) CT scans from eight patients at Yale New Haven Hospital. Four of these eight patients have an additional scan after surgical repair (postR). The PreD CT scans were originally performed as part of the patients' regular medical care, under the direction of their treating physicians, and were not specifically obtained for the purpose of this study.

Table 1: Patient Information

Patient ID	1	2	3	4	5	6	7	8
Age at first presentation	67	54	66	63	73	41	63	75
Sex	M	M	F	M	F	M	M	M
Height	163	170	163	163	160	175	188	188
Weight	120.5	80	55	49	62	72	100	109
Max Asc Diam	5.2	6	4.5	5.38	3.36	5.1	6.5	5.1
PreD CT Date	8/8/19	1/27/19	6/18/18	10/1/13	7/4/14	1/4/12	6/24/09	3/15/10
PostD CT Date	12/12/19	8/6/19	6/20/18	1/3/16	7/8/15	6/20/14	4/24/12	1/25/11
PostR CT Date	2/6/20	8/17/19	N/A	N/A	N/A	N/A	12/5/13	2/14/11

2.2 Patient-specific geometry reconstruction and meshing

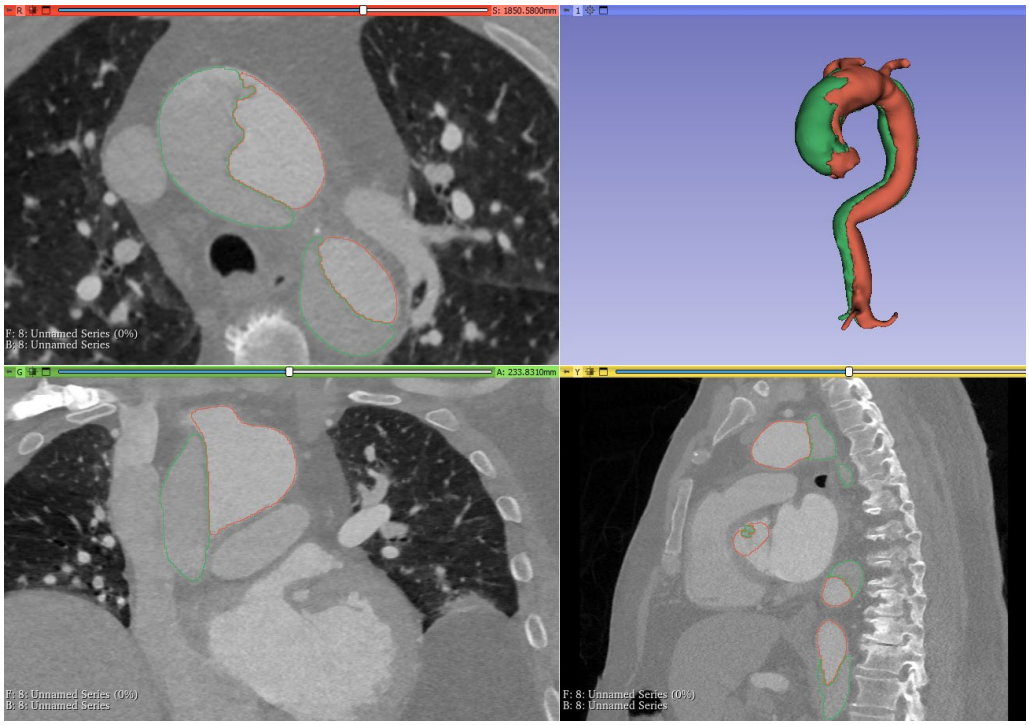

Figure 1: Reconstruction of patient-specific geometries based on MSCT data.

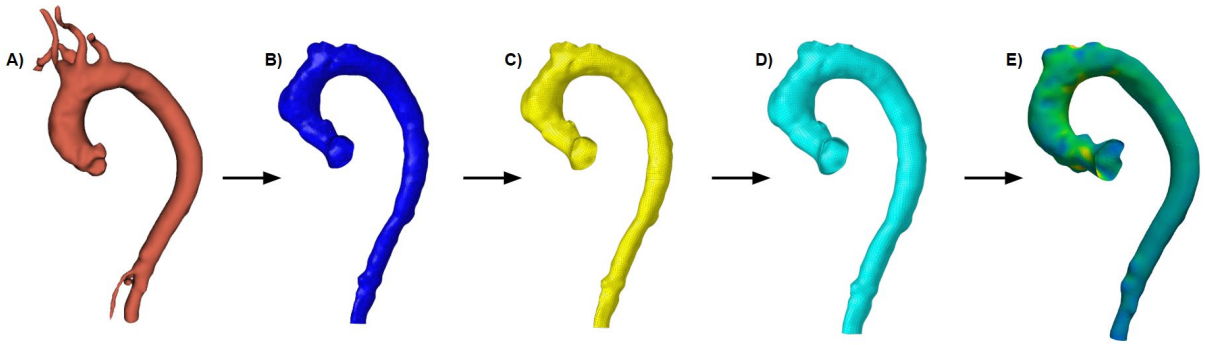

Figure 2: The procedure of stress analysis based on patient-specific geometries. A) 3D slicer model, B) Hypermesh surface, C) Hypermesh shell mesh, D) Element offset, E) FE stress analysis result.

The patient-specific geometries were segmented from CT images using 3D Slicer (www.slicer.org) software (Figure 1). The reconstructed geometries include the aortic root, ascending aorta, aortic arch, together with the 3 branches (the brachiocephalic artery, the left common carotid

artery and the left subclavian artery), the proximal and distal descending aorta, as well as the true lumen, false lumen, and dissection flaps (Figure 2A).

Finite element (FE) meshes were then generated using HyperMesh (Altair Engineering, Inc., MI) software. First, the surface geometries were generated based on the segmented patient-specific geometries (Figure 2B), then surface meshes with the 4-node quadrilateral shell elements were created (Figure 2C). Aortic wall solid meshes with four layers of 8-node brick elements were created by offsetting the surface meshes (Figure 2D). In this study, the thickness of aortic wall without dissection was assumed to be 2 mm, while the thickness of the dissection wall was assumed to be half of the normal thickness according to the observation of Dr. Elefteriades in clinics.

2.3 Finite element (FE) modeling for stress analysis

Finite Element (FE) modeling was performed using the Abaqus/Standard (SIMULIA, Providence, RI), based on Static Determinacy Approach (SDA). More details about the application of the SDA can be found in our previous publications.[20,21] Briefly, the static determinacy is a property of pressurized structures whose internal tension/stress is independent of the material properties (i.e. the tension/stress can be calculated based only on the external pressure/force and geometry).[21] Using Laplace's law to compute the wall hoop stress of a perfect cylindrical tube is one of the most well-known examples of static determinacy.[21] Though the geometry of the aorta is much more complex, it has been shown[21–23] that the aorta under a pressure loading can also be treated as a structure with static determinacy and that the aortic wall stress is independent of material properties[24–26] and can be calculated directly from the pressure and geometry.

Since the calculation of aortic wall stress does not need material properties under a quasi-static pressure loading condition, during the FE simulation, the simple isotropic linear elastic material properties of extremely large stiffness were applied to the aortic wall as done in our previous study.[23]

The nodal displacements were fixed at the boundaries of the aorta segments of interest, including the inlet of the ascending aorta (around the aortic annulus), outlet of the three branches, and outlet of the descending aorta. The systolic blood pressure was applied to the inner surface of the aorta, and the stress fields were calculated and analyzed (Figure 2E).

FE stress analysis was performed for each patient at pre-dissection (PreD) and post-dissection (PostD) states, as well as post-repair (PostR) state if data was available. To understand the impact of varying blood pressure levels on the aortic wall stresses, three systolic blood pressure values were utilized: 16 kPa (~120 mmHg), 18 kPa (~135 mmHg), and 20 kPa (~150 mmHg), which corresponded to normal systolic blood pressure, hypertension stage 1, and hypertension stage 2, respectively.[27]

Principal stresses were obtained for each element in the finite element mesh, and the one with the maximum absolute value (a.k.a. maximum absolute principal stress) was used in stress analysis throughout this study and was simply referred as stress. Because the aortic wall mesh is comprised of 4 layers of elements, the aortic wall stress is calculated as the averaged stress of the 4 layers of elements across the wall thickness. The aorta was segmented into five anatomic segments, i.e., the aortic root, ascending aorta, aortic arch, proximal descending aorta, and distal descending aorta (Figure 3). As clinically, dissections occur near the root area, the aortic root was further split into the non-coronary Sinus of Valsalva (NCS), left coronary sinus (LCS), and right coronary sinus (RCS), as shown in Figure 4. The mean stresses of all elements within the five anatomic segments of the aorta and the three segments of the aortic root were obtained, as a high mean stress would indicate that the entire segment is subject to high stress. The peak stresses, or the maximum stresses, of all elements within the five anatomic segments of the aorta and the three segments of the aortic root were also obtained and compared, as a high peak stress could indicate a concentrated “hotspot” of high stress, leading to a focal location of material failure.

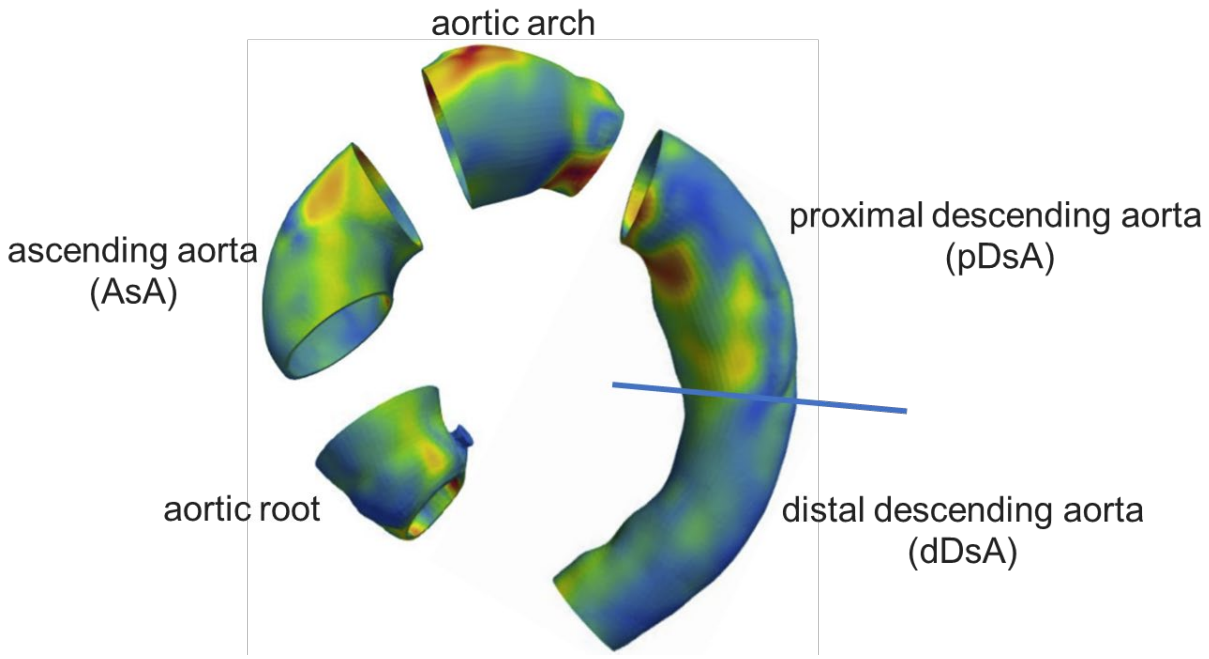

Figure 3: The five regions of the aorta: aortic root, ascending aorta, aortic arch, proximal descending aorta, and distal descending aort. Stress is color-coded.

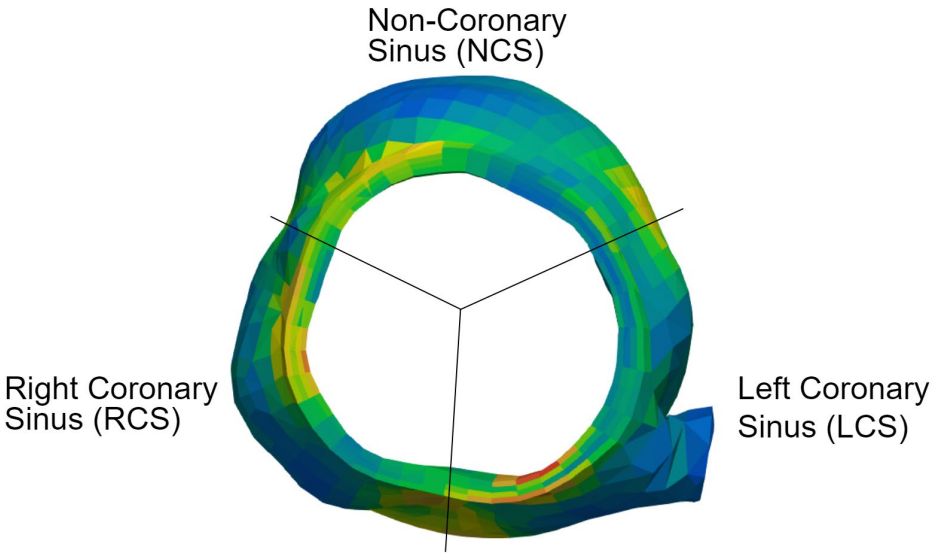

Figure 4: The three segments of the aortic root, viewed from the Sinuses of Valsalva to the sinotubular junction: left coronary sinus, right coronary sinus, and non-coronary sinus. The stress is color-coded.

Paired Student's t-tests were used to compare the differences in mean and peak stress between different states (preD, postD, and postR) and between different regions (in the aorta: Root, AsA, Arch, pDsA, and dDsA, and in the root: LCC, RCC, NCC). For comparisons against the PostR state, only patients who had

CT data from all three states were considered. For all statistical considerations, a p-value of < 0.05 was deemed to indicate a significant difference. All the data given in the following sections are presented as the mean ± standard deviation.

3. RESULTS

3.1 Stresses in the aortic wall at preD, postD, and postR states

The stress distributions in the aortic wall of a representative aorta at the preD, postD, and postR states under the normal physiological loading condition of 16 kPa are shown in Figure 5 for both anterior and posterior views of the aorta. As depicted in Figure 5A&D, the stress color map of the preD state clearly revealed stress concentration "hotspot" locations in the aortic wall. In the preD state (Figure 5A&D), the locations with high stress hotspots are the same as in the postD state, but these areas experience much higher stresses in the postD state. After surgical repair in postR, there is a significant decrease in the overall stress in the aorta, as seen in Figure 5C&F.

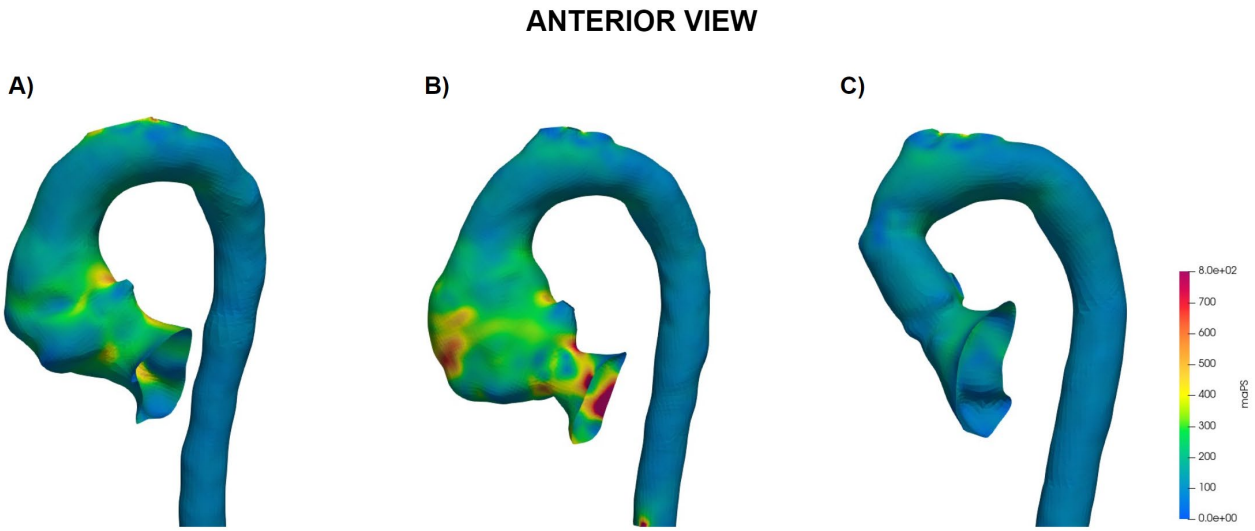

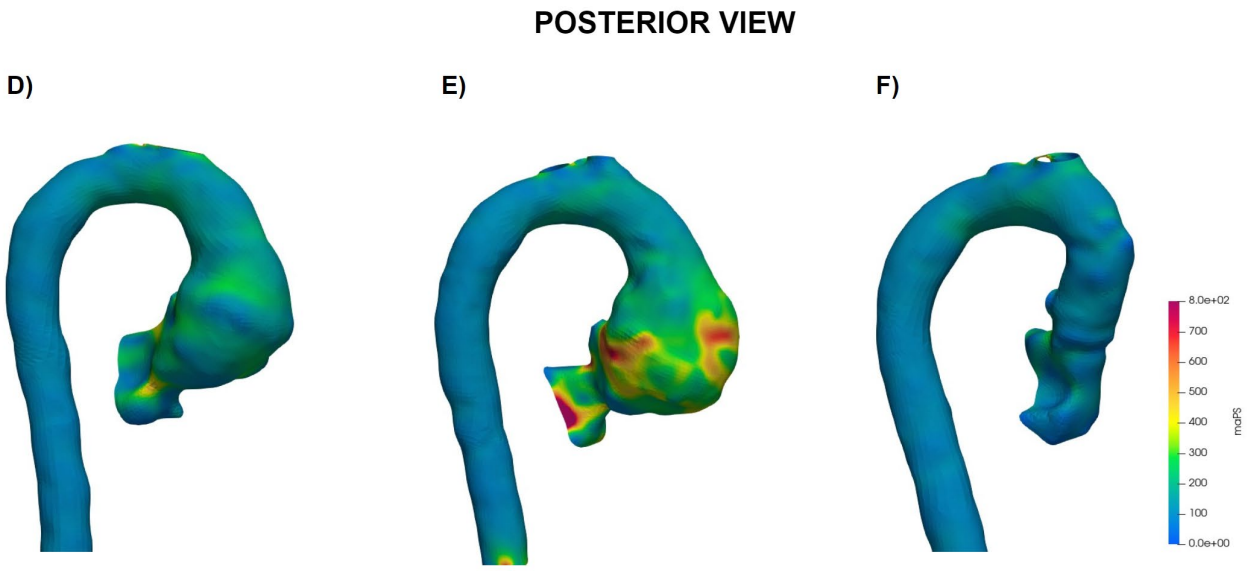

Figure 5: Anterior and posterior views of the aortic wall stress of a representative aorta

3.1.1 Mean stresses in the aortic wall at preD, postD, and postR states

The mean stresses in the five aorta regions, defined in Figure 3, all increased from the preD state to the postD state, and subsequently decreased after surgical repair (postR), as shown in Figure 6. For example, the mean stress of the aortic root in preD was 161.1±9.2 kPa, which significantly increased to 241.3±21.9 kPa in postD, and then significantly decreased to 141.8±9.6 kPa in postR. The mean stresses in the ascending aorta and aortic arch follow the same statistically significant trend. However, for the proximal and descending aorta, the mean stress in the proximal descending aorta was 115.5±4.8 kPa in preD, and significantly increased to 235.8±29.9 kPa in postD, and its mean stresses were reduced to 125.9±9.4 kPa in the postR state, but this reduction was not significantly reduced because the surgical repair procedure only operated on the ascending aorta segment. The same trend was observed in the distal descending aorta segment.

At all regions of the aorta, there was a significant difference (paired t-test, p-value < 0.05) between the preD and postD mean stresses. ~~For the aortic root, ascending aorta, and arch, there was also a~~

~~significant difference (paired t-test, p-value < 0.05) between the postD and postR states.~~ For all regions of the aorta, there was no significant difference between the preD and postR states, indicating that the repair surgery successfully restored the wall stress from an elevated stress state in postD to a hemostasis state in preD.

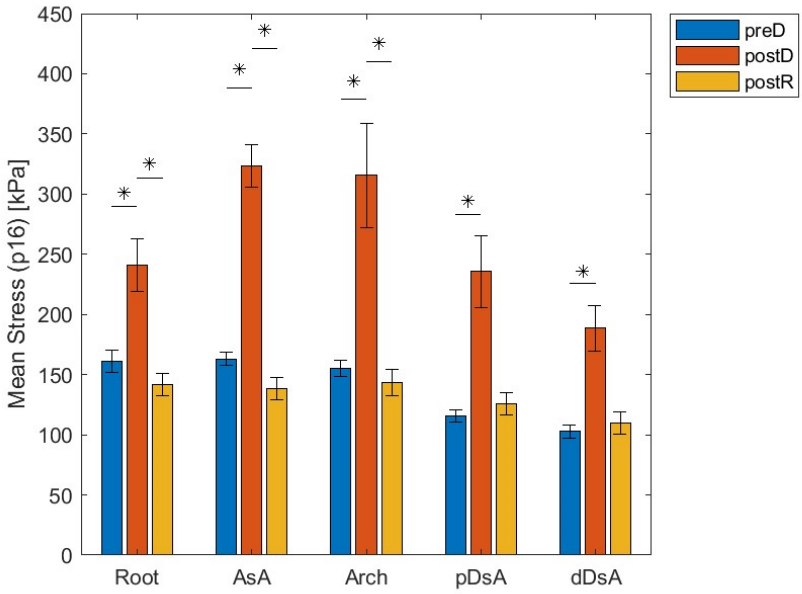

*Figure 6: Mean stresses of all patients in the PreD, PostD, and PostR states, separated by aortic regions. Note * indicates a statistically significant difference between two groups.*

3.1.2 Peak stresses in the aortic wall at preD, postD, and postR states

A similar trend occurred in the peak aortic wall stresses in all regions, as shown in Figure 7. In the Root, AsA, and pDsA, there was a significant difference (paired t-test, p-value < 0.05) in the peak stresses between the preD and postD, and between the postD and postR states. There were no significant differences in the peak stresses between the preD and postR states for all regions of the aorta. For example, the peak stresses in the aortic root at the preD state (370.8.7±35.2 kPa) increased to 681.9±100.2 kPa in the postD state, then decreased to 306.4±12.2 kPa at the postR state. The peak stress in the pDsA region was 230.6±13.8 kPa at the preD state, which significantly increased to 714.3±144.69 kPa in the postD

state, and subsequently reduced to 224.0±11.3 kPa in the postR state. However, this reduction in peak stress at the postR state again was not significantly different from the postD state, as the surgical repair procedure did not operate on the descending aorta. The dDsA also had a significant difference between the peak stresses of the preD and postD state, but not between the postD and postR states. Interestingly, there was no significant difference between peak stresses in the preD, postD, and postR states for the Arch. When comparing between the regions of the aorta at the preD state, we found that there was a significant difference in the peak stresses for all comparisons except one. There was no significant difference between the peak stresses of the Root and the AsA in the preD state.

Overall, the ascending aorta (consisting of three regions: Root, AsA, and Arch, see Figure 3) experienced higher mean and peak stresses than the descending aorta (pDsA and dDsA) in the preD and postR states. For example, in the preD state, the mean stress was 161.1 kPa in the Root, 162.9 kPa in the AsA region, and 155.2 in the Arch, whereas the mean stress was 155.5 kPa in the pDsA region, and 102.7 kPa in the dDsA region. Again, in the preD state, the peak stress was 370.8 kPa in the Root, 374.6 kPa in the AsA region, and 585.5 kPa in the Arch, whereas the peak stress is 230.6 kPa in the pDsA region and 145.4 kPa in the dDsA region.

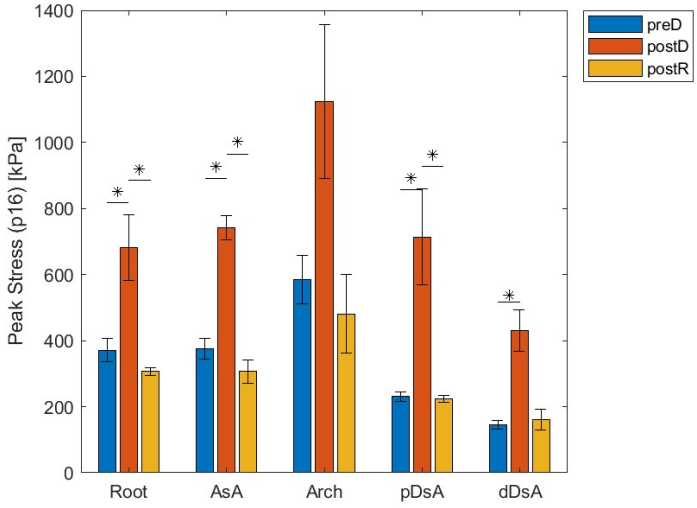

Figure 7: Peak stresses of all patients in the PreD, PostD, and PostR states, grouped by aortic regions.

3.2. Mean and peak stresses of the aortic root at preD, postD, and postR states

The FE results of the three aortic root sections (LCC, RCC, and NCC) can be seen in Figure 8. There was again a significant increase in mean stresses from the preD to the postD state, and the mean stresses decreased after surgical repair. In the preD state, the LCC, RCC and NCC had mean stresses of 173.4±13.9 kPa, 168.6±11.1 kPa, and 149.0±10.8 kPa, respectively. The NCC experienced the highest increase in stress from the preD to the postD states compared to the LCC and RCC, increasing an average of 111.6 kPa whereas the LCC increased 55.6 kPa, and the RCC increased 70.7 kPa.

For all regions of the aortic root, there was a significant difference in the mean stresses between the preD and postD states, and between the postD and postR states. For all regions, there was no significant difference in the mean stresses between the preD and postR states, an indication of successful surgical repair. There were also no significant differences between the mean stresses of the three regions in the preD state.

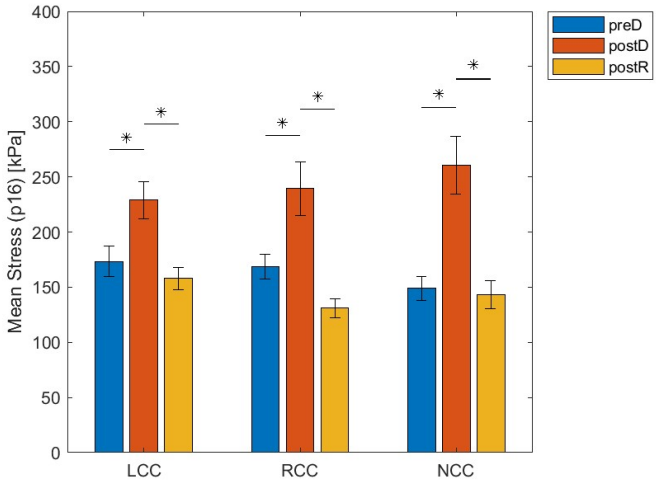

Figure 8: Mean stresses of all patients in the PreD, PostD, and PostR states, separated by aortic root regions.

When analyzing the peak stresses in the different regions of the aortic root, we found that there was an increase in peak stress between the preD and postD states, and a subsequent decrease in the peak stress between the postD and the postR states, as seen in Figure 9. For example, the LCC had a peak stress of 355.8 kPa±40.2 kPa in the preD state, increased to 562.5±51.4 kPa in the postD state, and reduced to 291.5±18.5 kPa in the postR state. There was a significant difference in the peak stresses between the preD and postD states in the LCC and NCC, and there was a significant difference in the peak stresses between the postD and postR states in the LCC and RCC. There was no significant difference in the peak stresses between the preD and postR states in all 3 aortic root sections, indicating, again, the surgical repair successfully restored the preD peak stress state.

In the preD state, there is no significant difference in the peak stresses between the LCC and RCC and between the LCC and NCC, but there is a significant difference in the peak stresses between the RCC and NCC.

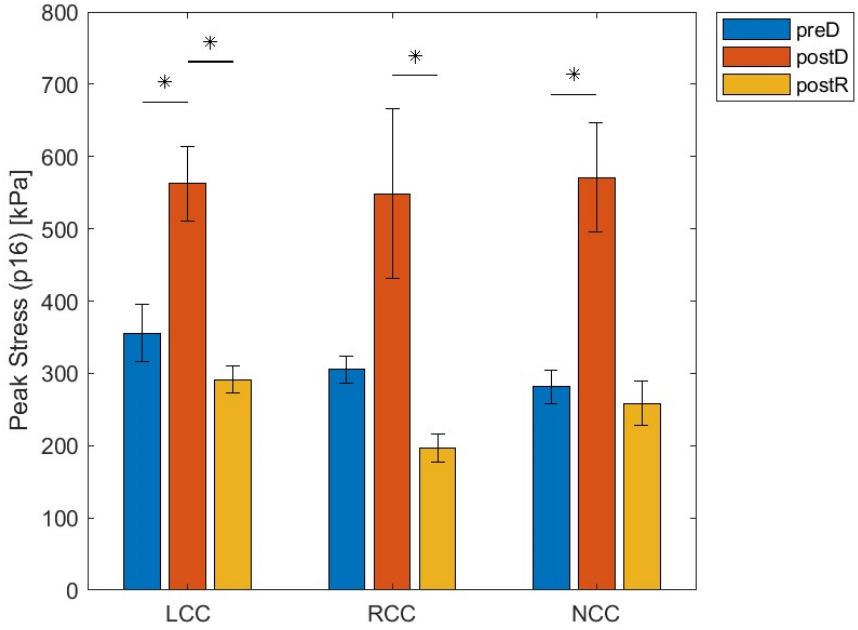

Figure 9: Peak stresses of all patients in the PreD, PostD, and PostR states, grouped by aortic root regions.

3.3. Mean and peak stresses of the aorta and the aortic root under hypertensive systolic pressure of 18 kPa and 20 kPa.

We further obtained and compared the mean and peak stresses in different regions of the aorta and the aortic root under hypertensive systolic pressures of 18 kPa (hypertension stage-1) and 20 kPa (hypertension stage-2). A representative aorta at the postD state is illustrated in Figure 10, in which Figure 9A&D show anterior and posterior views of true and false lumens, and the remaining 4 columns show the stresses on the aortic wall under pressure levels of 16 kPa, 18 kPa, and 20 kPa, respectively.

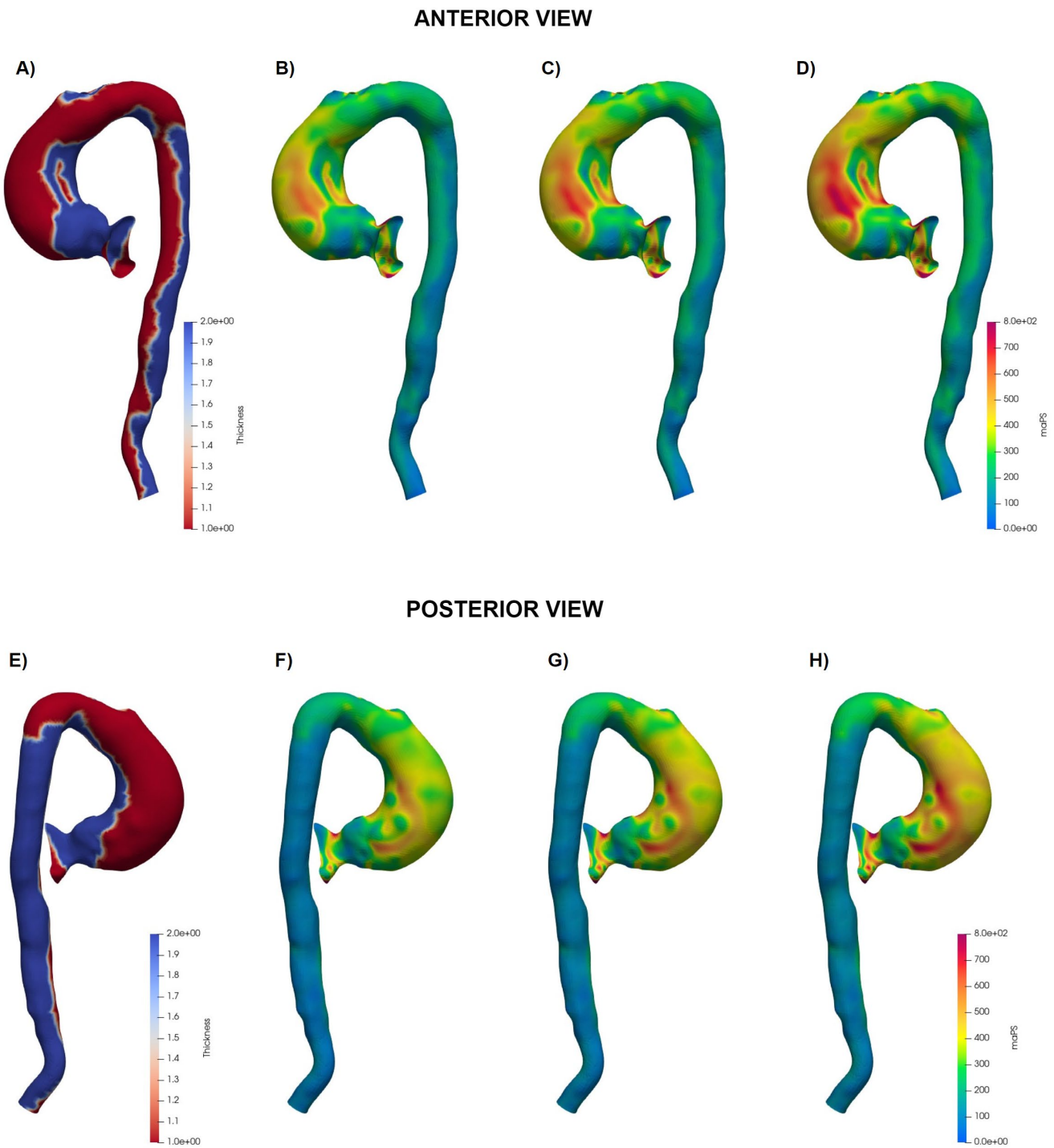

Figure 10: Anterior and posterior views of the stress map of a representative aorta at the postD state at 16, 18, and 20 kPa.

There were three differences between the normal systolic pressure condition of 16 kPa and the hypertension states. (1) Under 16 kPa pressure, there was no significant difference in any of the regions

for mean or peak stresses between the preD and postR states. However, in the hypertension conditions, there was a significant difference between the mean stresses of the preD and postR states in the AsA region. (2) In the hypertension conditions (18 and 20 kPa), there was no significant difference between the mean stresses in the postD and postR states in the Arch, but there was a significant difference under a normal systolic blood pressure. (3) Lastly, in the hypertension stage-2 condition (20 kPa), there was a significant difference in the maximum stresses of the RCC between the preD and postD states, whereas there was no significant difference in lower blood pressure conditions.

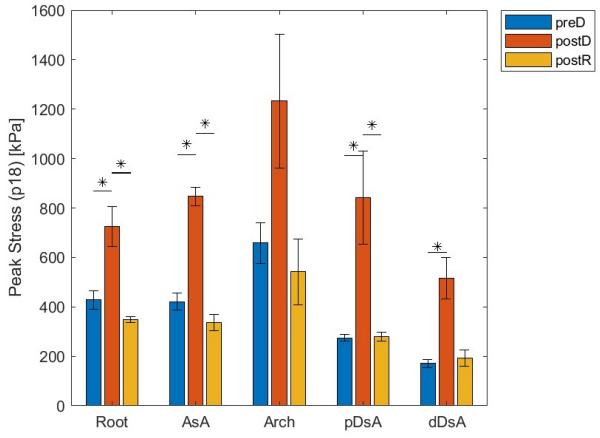

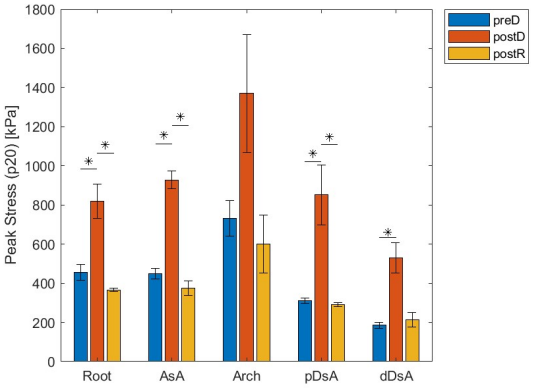

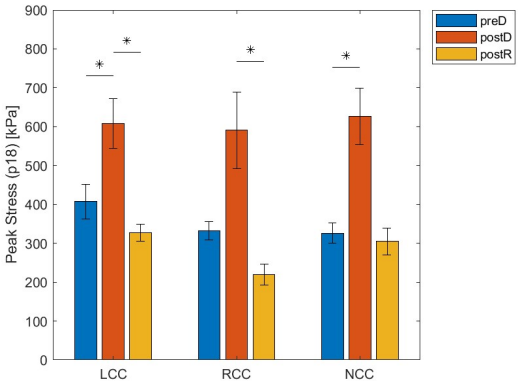

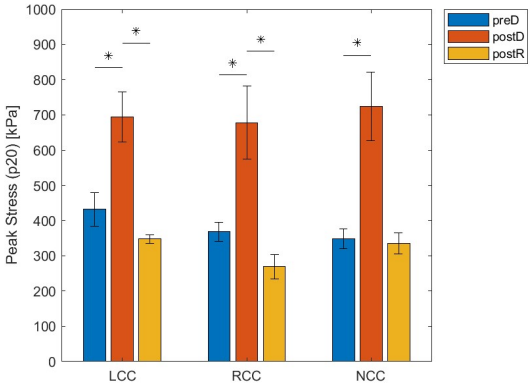

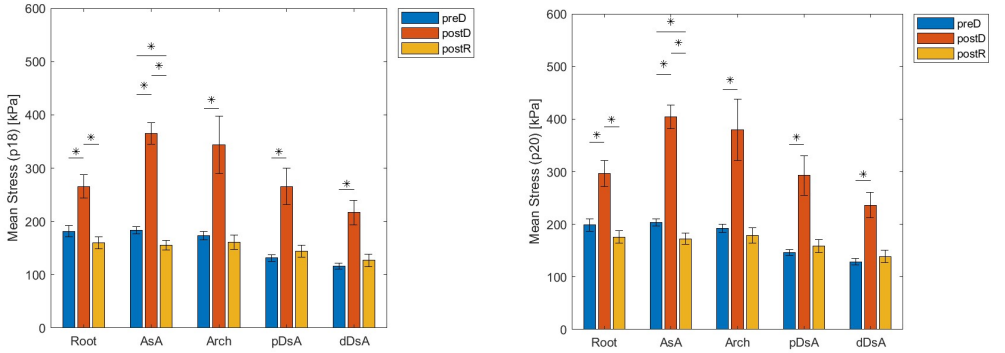

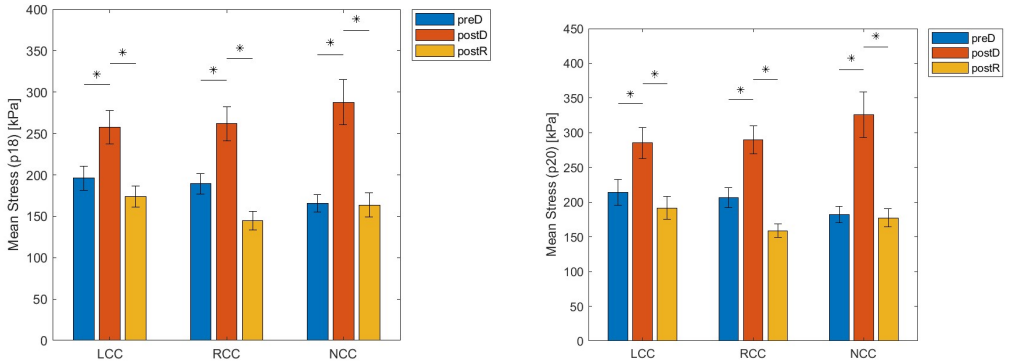

4. DISCUSSION

4.1. High aortic wall stress at the post-dissection state (necessity of surgery)

Using 120mmHg (16 kPa) as the normal systolic blood pressure, the stresses at the postD state are significantly higher than those at the preD and postR states. For example, the mean stress in the AsA region was 162.9±5.6 kPa at the preD state, 323.6±17.8 kPa at the postD state, and 138.0±9.1 kPa at the postR state under the 120mmHg systolic blood pressure. The standard deviation was calculated across different patients. The increase in stress leads to increased risk of rupture. To quantify the risk of rupture, we calculated the probability index of rupture, which was developed in our previous work,[28] and the aneurysm rupture probability of each of the eight patients is higher than 0.9, indicating imminent rupture if left untreated.

4.2. Surgical repair restores the aortic wall stress to a normal state (effectiveness of surgery)

Using 120mmHg (16 kPa) as the normal systolic blood pressure, we found that there was no significant difference between the postR and the preD stresses at all sections of the aorta and aortic root for both mean and peak stresses. This indicates that the surgical repair is effective and restores aortic stress of a patient with aortic dissection back to the pre-dissection state across all regions of the aorta. Interestingly, even though surgical repair only alters the geometry of the ascending aorta and leaves the Root and Arch, descending aorta intact, the mean stresses of all sections of the Root (LCC, NCC, and RCC) and the Arch significantly decrease.

In hypertension conditions, there was a significant difference between the mean stresses at the preD and postR states in the AsA. From the data, the mean stress was lower in the postR state (155.1±9.3 at 18 kPa and 172.7±11.0 at 20 kPa) than the preD state (183.3±6.4 at 18 kPa and 203.5±6.6 at 20 kPa). Surgical repair not only restores the preD stress state across all regions, but it also allows for the ascending aorta to better tolerate high blood pressure conditions.

4.3 Comparing between sections/regions of the aorta in preD state.

At preD state in normal systolic pressure (16 kPa), root and AsA had the same mean and peak stresses. The entire ascending aorta experiences higher pressure than the descending aorta, mostly because the diameter of the ascending aorta is much larger than the diameter of the ascending aorta.

At the normal systolic pressure and the preD state, there was no significant difference between the mean stresses of the Root, AsA (ascending aorta), and Arch. When averaged across the entire area of each region, the stresses that the entire ascending aorta (including the root, AsA, and Arch regions) were not significantly different from each other, and the mean stresses in these three areas were consistently higher than those in the descending aorta (including the pDsA and the dDsA). However,

when comparing the peak stresses, only the root and the AsA had no significant difference. At a normal systolic blood pressure condition before dissection, the root and the AsA regions experienced the same average and maximum stresses.

We observed that high curvature at arch caused high stress. While there was no significantly different average stress between the root and AsA, the peak stresses in the arch were significantly higher than those in both the root and the AsA. This is likely because of the sharp curvature caused by the aortic branches in the Arch region, which will lead to a higher stress in the aortic wall in areas where there is a sharp change in geometry.

Except the Arch, all other regions had a significant increase in peak stress between the preD and postD states. The mean stress of the Arch followed the same trend as the other regions and significantly increased from the preD to postD states. Given this observation, it could mean that the sharp curves in the geometry of the aortic arch create such a high stress that the dissection doesn't increase the stress by a significant amount even though the overall stresses increase.

4.4 Possible correlation between dissection and high stress spots

From the FE stress analysis, at the 16 kPa (120mmHg) physiological loading condition, the mean stress in the PreD state is 161.1±9.2 kPa in the aortic root, 162.9±5.6 kPa in the ascending aorta, and 155.2±6.8 kPa in the aortic arch. The mean stresses in these three regions were significantly higher ($p < 0.001$) compared to the descending aorta, which had a mean stress of 111.2±4.8 kPa in the proximal descending aorta and 102.7±5.2 kPa in the distal descending aorta.

Furthermore, we identified stress concentration regions by defining them as areas with stress values greater than the 75th percentile in the aortic wall. Interestingly, for one of the patients, these high-

stress regions exhibited strong correlations with the actual dissection borders observed in patients at the post-dissection stage (Figure 11).

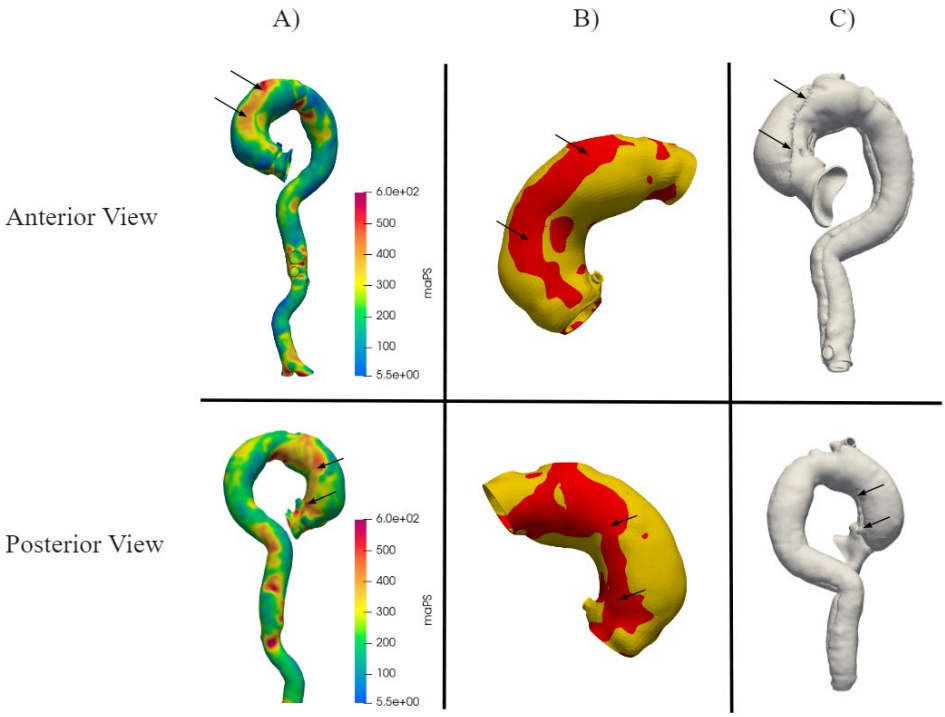

Figure 11: Anterior and posterior views of a representative aorta with (A) the PreD stress distribution, (B) a threshold image of just the ascending aorta, where the red region represents the stresses greater than the 75th percentile, and (C) the PostD state. The arrows show areas of stress concentration and the dissection borders. For a better visualization, two separate meshes are used for the true and false lumens in (C).

4.5 Limitation and future work

This study has several limitations, and we intend to resolve the limitations in our future work. Firstly, the wall thickness was assumed to be uniform (the thickness of aortic wall without dissection was assumed to be 2 mm, while the thickness of the dissection wall was set to be half of the normal value according to clinical observations from Dr. Elefteriades. Prior reports have shown that the aortic arch has a wide variation in wall thickness, and there is a thicker wall in the sharp curves between aortic branches.[29] This thicker wall of aorta arch would act as a natural reinforcement to reduce the high peak stresses we observed in the simulation, and it is likely that the true stresses in the aortic arch are lower than the calculated stresses by FEA. More accurate wall thickness can be obtained by using both the contrast and

non-contrast CT images: the inner wall will be revealed by the contrast CT image, and the outer wall will be revealed by the non-contrast CT image. Secondly, the normal systolic pressure was assumed to be a fixed number, instead of a range of feasible pressure values. An interesting future study could be the investigation of rupture probability when the normal pressure is less than 120mmHg, which could provide useful information for blood pressure control to avoid rupture while waiting for surgery. This study did not investigate dissection progression. To investigate dissection progression after a dissection tear occurs, the Fluid-structure interaction (FSI) approach could be used. However, it would be difficult to obtain image data at the dissection tear formation state. In addition, our future work will include machine learning-based FEA to facilitate a fast and accurate estimate of aortic wall stress and allow for patient-specific diagnosis and prediction of aortic dissection/rupture.

5. CONCLUSIONS

We performed patient-specific stress analysis of aortic dissection at three time points: preD, postD, and postR. By analyzing mean and peak stress values across different regions and states, we observe distinct patterns that highlight the mechanical response of the aorta to dissection and subsequent repair.

ACKNOWLEDGEMENTS

This study was supported in part by the NIH grant R01 HL158829.

CONFLICT OF INTEREST STATEMENT

Christina Sun, Tongran Qin, and Wei Sun are stakeholders of Sutra Medical Inc. No other conflicts were reported.

APPENDIX

Table 2: Mean stress at each region of the aorta at 120 mmHg pressure.

Aorta Region	preD stress (kPa)	postD stress (kPa)	postR stress (kPa)
Root	161.1 ± 9.2	241.3 ± 21.9	141.8 ± 9.6
AsA	162.9 ± 5.6	323.6 ± 17.8	138.0 ± 9.1
Arch	155.2 ± 6.8	315.5 ± 43.1	143.3 ± 11.0
pDsA	115.2 ± 4.8	235.8 ± 29.9	125.9 ± 9.4
dDsA	102.7 ± 5.2	188.5 ± 19.3	109.7 ± 9.4

Table 3: Mean stress at each region of the aortic root at 120 mmHg pressure.

Aortic Root Region	preD stress (kPa)	postD stress (kPa)	postR stress (kPa)
LCS	173.4 ± 13.9	229.0 ± 16.9	157.9 ± 10.2
RCS	168.6 ± 11.1	239.3 ± 24.4	130.9 ± 8.8
NCS	149.0 ± 10.8	260.5 ± 26.4	143.2 ± 12.7

Table 4: Peak stress at each region of the aorta at 120 mmHg pressure.

Aorta Region	preD stress (kPa)	postD stress (kPa)	postR stress (kPa)
Root	370.8 ± 35.2	681.9 ± 100.2	306.4 ± 12.2
AsA	374.6 ± 31.5	742.4 ± 36.1	306.4 ± 34.6
Arch	585.5 ± 73.1	1123.5 ± 233.6	481.4 ± 118.1
pDsA	230.6 ± 13.8	714.3 ± 144.7	224.0 ± 11.3
dDsA	145.4 ± 13.7	430.4 ± 61.7	161.0 ± 31.9

Table 5: Peak stress at each region of the aortic root at 120 mmHg.

Aortic Root Region	preD stress (kPa)	postD stress (kPa)	postR stress (kPa)
LCS	173.4 ± 13.9	229.0 ± 16.9	157.9 ± 10.2
RCS	168.6 ± 11.1	239.3 ± 24.4	130.9 ± 8.8
NCS	149.0 ± 10.8	260.5 ± 26.4	143.2 ± 12.7

Table 6: Mean stress at each region of the aorta at 135 mmHg pressure.

Aorta Region	preD stress (kPa)	postD stress (kPa)	postR stress (kPa)
Root	181.5 ± 10.5	265.5 ± 22.0	159.4 ± 11.2
AsA	183.3 ± 6.4	364.7 ± 20.4	155.1 ± 9.3
Arch	173.6 ± 7.8	343.4 ± 53.7	160.8 ± 13.3
pDsA	131.2 ± 5.7	265.5 ± 34.3	143.7 ± 11.1

dDsA	115.9 ± 5.8	216.5 ± 22.9	126.8 ± 11.6

Table 7: Mean stress at each region of the aortic root at 135 mmHg pressure.

Aortic Root Region	preD stress (kPa)	postD stress (kPa)	postR stress (kPa)
LCS	196.0 ± 14.3	257.6 ± 20.5	174.0 ± 12.5
RCS	189.3 ± 12.5	261.8 ± 20.7	144.7 ± 11.0
NCS	165.6 ± 10.6	287.7 ± 27.2	163.7 ± 14.4

Table 8: Peak stress at each region of the aorta at 135 mmHg pressure.

Aorta Region	preD stress (kPa)	postD stress (kPa)	postR stress (kPa)
Root	428.1 ± 37.3	724.6 ± 81.0	348.7 ± 12.9
AsA	421.4 ± 35.5	847.0 ± 37.1	335.7 ± 33.1
Arch	658.7 ± 82.3	1232.8 ± 270.5	541.5 ± 132.8
pDsA	274.2 ± 13.0	842.6 ± 189.1	279.1 ± 18.4
dDsA	170.8 ± 16.3	516.0 ± 84.1	193.1 ± 32.8

Table 9: Peak stress at each region of the aortic root at 135 mmHg pressure.

Aortic Root Region	preD stress (kPa)	postD stress (kPa)	postR stress (kPa)
LCS	407.1 ± 43.8	608.5 ± 63.5	326.6 ± 21.9
RCS	332.7 ± 23.2	590.8 ± 98.6	219.3 ± 27.0
NCS	326.0 ± 26.2	626.8 ± 72.0	304.7 ± 35.1

Table 10: Mean stress at each region of the aorta at 150 mmHg pressure.

Aorta Region	preD stress (kPa)	postD stress (kPa)	postR stress (kPa)
Root	198.6 ± 12.0	296.5 ± 24.4	176.0 ± 12.0
AsA	203.5 ± 6.6	404.5 ± 22.1	172.7 ± 10.9
Arch	192.5 ± 8.3	379.7 ± 58.5	178.7 ± 14.3
pDsA	146.2 ± 5.8	292.9 ± 37.7	158.4 ± 12.5
dDsA	128.6 ± 6.4	236.2 ± 24.1	138.7 ± 11.7

Table 11: Mean stress at each region of the aortic root at 150 mmHg pressure.

Aortic Root Region	preD stress (kPa)	postD stress (kPa)	postR stress (kPa)
LCS	241.2 ± 18.5	285.2 ± 22.3	191.6 ± 16.5
RCS	206.3 ± 14.5	289.8 ± 20.0	158.9± 9.6
NCS	182.2 ± 12.0	325.8 ± 32.6	177.3 ± 13.0

Table 12: Peak stress at each region of the aorta at 150 mmHg pressure.

Aorta Region	preD stress (kPa)	postD stress (kPa)	postR stress (kPa)
Root	455.7 ± 40.5	820.1 ± 87.3	366.3 ± 7.4
AsA	448.9 ± 26.0	927.5 ± 45.1	374.2 ± 37.5
Arch	731.8 ± 91.4	1369.5 ± 300.3	601.7 ± 147.6
pDsA	310.5 ± 14.2	851.7 ± 153.7	291.2 ± 10.5
dDsA	185.8 ± 14.8	529.2 ± 76.9	214.5 ± 36.7

Table 13: Peak stress at each region of the aortic root at 150 mmHg.

Aortic Root Region	preD stress (kPa)	postD stress (kPa)	postR stress (kPa)
LCS	431.8 ± 47.1	695.3 ± 71.1	348.0 ± 12.0
RCS	368.6 ± 27.6	678.3 ± 103.9	269.7 ± 34.5
NCS	349.3 ± 28.1	724.2 ± 97.5	335.7 ± 29.3

1. Hagan PG, Nienaber CA, Isselbacher EM, et al. The International Registry of Acute Aortic Dissection (IRAD)New Insights Into an Old Disease. *JAMA*. 2000;283(7):897-903. doi:10.1001/jama.283.7.897

2. Gawinecka J, Schönrath F, von Eckardstein A. Acute aortic dissection: pathogenesis, risk factors and diagnosis. *Swiss Med Wkly*. 2017;147:w14489. doi:10.4414/smw.2017.14489

3. Gudbjartsson T, Ahlsson A, Geirsson A, et al. Acute type A aortic dissection – a review. *Scandinavian Cardiovascular Journal*. 2020;54(1):1-13. doi:10.1080/14017431.2019.1660401

4. Jassar AS, Sundt TM. How should we manage type A aortic dissection? *Gen Thorac Cardiovasc Surg*. 2019;67(1):137-145. doi:10.1007/s11748-018-0957-3

5. Mészáros I, Mórocz J, Szlávi J, et al. Epidemiology and clinicopathology of aortic dissection. *Chest*. 2000;117(5):1271-1278. doi:10.1378/chest.117.5.1271

6. Tran TP, Khoynezhad A. Current management of type B aortic dissection. *Vascular Health and Risk Management*. 2009;5:53-63. doi:10.2147/vhrm.s12187454

7. Levy D, Goyal A, Grigorova Y, Farci F, Le JK. Aortic Dissection. In: *StatPearls*. StatPearls Publishing; 2023. Accessed October 1, 2023. http://www.ncbi.nlm.nih.gov/books/NBK441963/

8. Nienaber CA, Clough RE. Management of acute aortic dissection. *The Lancet*. 2015;385(9970):800-811. doi:10.1016/S0140-6736(14)61005-9

9. Hiratzka LF, Bakris GL, Beckman JA, et al. 2010 ACCF/AHA/AATS/ACR/ASA/SCA/SCAI/SIR/STS/SVM Guidelines for the diagnosis and management of patients with thoracic aortic disease. A Report of the American College of Cardiology Foundation/American Heart Association Task Force on Practice Guidelines, American Association for Thoracic Surgery, American College of Radiology,American Stroke Association, Society of Cardiovascular Anesthesiologists, Society for Cardiovascular Angiography and Interventions, Society of Interventional Radiology, Society of Thoracic Surgeons,and Society for Vascular Medicine. *J Am Coll Cardiol*. 2010;55(14):e27-e129. doi:10.1016/j.jacc.2010.02.015

10. Erbel R, Aboyans V, Boileau C, et al. 2014 ESC Guidelines on the diagnosis and treatment of aortic diseases: Document covering acute and chronic aortic diseases of the thoracic and abdominal aorta of the adult. The Task Force for the Diagnosis and Treatment of Aortic Diseases of the European Society of Cardiology (ESC). *Eur Heart J*. 2014;35(41):2873-2926. doi:10.1093/eurheartj/ehu281

11. Pape LA, Tsai TT, Isselbacher EM, et al. Aortic Diameter ≥5.5 cm Is Not a Good Predictor of Type A Aortic Dissection. *Circulation*. 2007;116(10):1120-1127. doi:10.1161/CIRCULATIONAHA.107.702720

12. LeMaire SA, Russell L. Epidemiology of thoracic aortic dissection. *Nat Rev Cardiol*. 2011;8(2):103-113. doi:10.1038/nrcardio.2010.187

13. Sherifova S, Holzapfel and GA. Biochemomechanics of the thoracic aorta in health and disease. *Prog Biomed Eng*. 2020;2(3):032002. doi:10.1088/2516-1091/ab9a29

14. Sherifova S, Holzapfel GA. Biomechanics of aortic wall failure with a focus on dissection and aneurysm: A review. *Acta Biomater*. 2019;99:1-17. doi:10.1016/j.actbio.2019.08.017

15. Bäumler K, Vedula V, Sailer AM, et al. Fluid–structure interaction simulations of patient-specific aortic dissection. *Biomech Model Mechanobiol*. 2020;19(5):1607-1628. doi:10.1007/s10237-020-01294-8

16. Martufi G, Di Martino ES, Amon CH, Muluk SC, Finol EA. Three-Dimensional Geometrical Characterization of Abdominal Aortic Aneurysms: Image-Based Wall Thickness Distribution. *Journal of Biomechanical Engineering*. 2009;131(061015). doi:10.1115/1.3127256

17. He X, Avril S, Lu J. Prediction of local strength of ascending thoracic aortic aneurysms. *Journal of the Mechanical Behavior of Biomedical Materials*. 2021;115:104284. doi:10.1016/j.jmbbm.2020.104284

18. Nathan DP, Xu C, Gorman JH, et al. Pathogenesis of acute aortic dissection: a finite element stress analysis. *Ann Thorac Surg*. 2011;91(2):458-463. doi:10.1016/j.athoracsur.2010.10.042

19. Li AE, Kamel I, Rando F, et al. Using MRI to Assess Aortic Wall Thickness in the Multiethnic Study of Atherosclerosis: Distribution by Race, Sex, and Age. *American Journal of Roentgenology*. 2004;182(3):593-597. doi:10.2214/ajr.182.3.1820593

20. Dong H, Liu M, Qin T, et al. Engineering analysis of aortic wall stress and root dilatation in the V-shape surgery for treatment of ascending aortic aneurysms. *Interactive CardioVascular and Thoracic Surgery*. 2022;34(6):1124-1131. doi:10.1093/icvts/ivac004

21. Liu M, Liang L, Liu H, Zhang M, Martin C, Sun W. On the computation of in vivo transmural mean stress of patient-specific aortic wall. *Biomech Model Mechanobiol*. 2019;18(2):387-398. doi:10.1007/s10237-018-1089-5

22. Joldes GR, Miller K, Wittek A, Doyle B. A simple, effective and clinically applicable method to compute abdominal aortic aneurysm wall stress. *Journal of the Mechanical Behavior of Biomedical Materials*. 2016;58:139-148. doi:10.1016/j.jmbbm.2015.07.029

23. Liu M, Liang L, Sun W. A new inverse method for estimation of in vivo mechanical properties of the aortic wall. *J Mech Behav Biomed Mater*. 2017;72:148-158. doi:10.1016/j.jmbbm.2017.05.001

24. Holzapfel GA, Gasser TC, Ogden RW. A New Constitutive Framework for Arterial Wall Mechanics and a Comparative Study of Material Models. *Journal of Elasticity*. 2000;61(1):1-48. doi:10.1023/A:1010835316564

25. Gasser TC, Ogden RW, Holzapfel GA. Hyperelastic modelling of arterial layers with distributed collagen fibre orientations. *J R Soc Interface*. 2006;3(6):15-35. doi:10.1098/rsif.2005.0073

26. Dong H, Sun W. A novel hyperelastic model for biological tissues with planar distributed fibers and a second kind of Poisson effect. *Journal of the Mechanics and Physics of Solids*. 2021;151:104377. doi:10.1016/j.jmps.2021.104377

27. Whelton PK, Carey RM, Aronow WS, et al. 2017 ACC/AHA/AAPA/ABC/ACPM/AGS/APhA/ASH/ASPC/NMA/PCNA Guideline for the Prevention, Detection, Evaluation, and Management of High Blood Pressure in Adults: A Report of the American College of Cardiology/American Heart Association Task Force on Clinical Practice Guidelines. *Hypertension*. 2018;71(6). doi:10.1161/HYP.0000000000000065

28. Liu M, Liang L, Zou Q, et al. A probabilistic and anisotropic failure metric for ascending thoracic aortic aneurysm risk assessment. *Journal of the Mechanics and Physics of Solids*. 2021;155:104539. doi:10.1016/j.jmps.2021.104539

29. Genovese K, Humphrey JD. Multimodal optical measurement in vitro of surface deformations and wall thickness of the pressurized aortic arch. *JBO*. 2015;20(4):046005. doi:10.1117/1.JBO.20.4.046005